

Stellar Dynamics around Black Holes in Galactic Nuclei

S. Sridhar^{*} and J. Touma[†]

^{*} *Inter-University Centre for Astronomy and Astrophysics, Ganeshkhind, Pune 411 007, INDIA*

[†] *University of Texas, McDonald Observatory, RLM 15.308, Austin, Texas, 78712*

8 March 2022

ABSTRACT

We classify orbits of stars that are bound to central black holes in galactic nuclei. The stars move under the combined gravitational influences of the black hole and the central star cluster. Within the sphere of influence of the black hole, the orbital periods of the stars are much shorter than the periods of precession. We average over the orbital motion and end up with a simpler problem and an extra integral of motion: the product of the black hole mass and the semimajor axis of the orbit. *Thus the black hole enforces some degree of regularity in its neighborhood.* Well within the sphere of influence, (i) planar, as well as three dimensional, axisymmetric configurations—both of which could be lopsided—are integrable, (ii) fully three dimensional clusters with no spatial symmetry whatsoever must have semi-regular dynamics with two integrals of motion. Similar considerations apply to stellar orbits when the black hole grows adiabatically. We introduce a family of planar, non-axisymmetric potential perturbations, and study the orbital structure for the harmonic case in some detail. In the centered potentials there are essentially two main families of orbits: the familiar loops and lenses, which were discussed in Sridhar and Touma (1997, MNRAS, 287, L1-L4). We study the effect of lopsidedness, and identify a family of loop orbits, whose orientation reinforces the lopsidedness, an encouraging sign for the construction of self-consistent models of eccentric, discs around black holes, such as in M31 and NGC 4486B.

Key words: galaxies: kinematics and dynamics

1 INTRODUCTION

Following up on a decade of work with ground-based telescopes (cf. Kormendy 1982, 1987 and Lauer 1983, 1985), observations with the Hubble Space Telescope (HST) have clarified, and extended our knowledge of the centres of galaxies (cf. Lauer et. al 1995, Gebhardt et al. 1996). The brightness profiles are generically cuspy, and many correlations have been drawn between cusp steepness, isophote shapes, luminosities, kinematics, and other nuclear and global properties of galaxies. Most, if not all, galaxies might have central black holes (BH), massive enough to power active nuclei when there is an adequate supply of fuel (Rees 1990). About a dozen galaxies have been shortlisted as candidates for possessing central BHs (c.f. Kormendy and Richstone 1995), and the case appears strong for our Galaxy, M31, M32, and NGC 3115. BH detection based on spectroscopy of stellar light requires careful modeling of the distribution and motions of stars in the central regions. Set against this background of progress, our understanding of the dynamics of

nuclear star clusters is quite poor. Gerhard and Binney (1985) argued that cusps and BHs will destroy box orbits, which are then replaced by chaotic orbits. The chaotic orbits being rounder, it is difficult to construct strongly non-axisymmetric equilibria (c.f. Merritt 1997, 1998 for a flavour of recent work in this area). Sridhar and Touma (1997) constructed, cuspy, non-axisymmetric, scale-free discs whose potentials are of Stäckel form in parabolic coordinates. The dynamics in these potentials is fully integrable. A BH could be added at the centre without affecting the integrability of motion. Discs without a BH support only “banana” orbits. The BH stabilizes a box-like family of orbits, the lenses. These models, as they questioned the implicit assumption that cusps and BHs imply chaos, perked our interest in further investigating dynamics very close to the BH. Here, we explore another route to more regular dynamics in galactic nuclei.

The orbits of stars in galactic nuclei are controlled by the combined gravitational forces of the central BH, and the self gravity of the cluster. Very close to the BH, the orbits are nearly Keplerian—stars bound to the BH move on nearly elliptical orbits, whereas very energetic ones follow hyperbolic trajectories (we ignore relativistic effects, so our discussion

^{*} E-mail: sridhar@iucaa.ernet.in

[†] E-mail: touma@harlan.as.utexas.edu

is applicable only to distances beyond several Schwarzschild radii from the BH). If the velocity dispersion in the cluster is σ , we might say that a BH of mass M has a strong influence on stellar orbits inside a sphere of radius, $r_h \sim GM/\sigma^2$. For fiducial values, $M \sim 10^8 M_\odot$, $\sigma \sim 100 \text{ km s}^{-1}$, we obtain $r_h \sim 50 \text{ pc}$, a spatial scale that HST with a resolution of $0.''1$ can easily resolve much farther than the Virgo cluster.[‡] Keplerian ellipses do not precess, and we might expect that orbits that are strongly influenced by the BH might support asymmetric, even lopsided structures. Such appears to be the case for M31 and NGC4486B, both of which have double nuclei (Lauer et.al. 1993, 1996); these might be signatures of eccentric nuclear stellar discs (Tremaine 1995). A few other galaxies with central asymmetric light distributions are discussed in Lauer et.al. (1995). As Lauer et.al. (1996) observe, “A thorough understanding of the dynamics of eccentric disks might allow us to estimate the BH mass directly from the disk shape by relating the scale at which the disc symmetry is broken to the hole mass.”

In this paper, we develop a perturbative approach toward classification of orbits within the BH sphere of influence, taking advantage of the super-integrability (i.e. degeneracy) of the Kepler problem. Borrowing an averaging technique from planetary dynamics, we introduce slow dynamics of precessional motions in § 2, and discuss integrability of slow dynamics in two, and three dimensional motions, for both time independent potentials, as well as the case when the mass of the BH grows adiabatically. We introduce a family of planar potentials that are, in general, cuspy, non-axisymmetric and lopsided. The harmonic case is particularly suited to simple, analytic treatment, and we devote § 3 to an exploration of orbits in non-axisymmetric, and lopsided cases; orbit families that might have relevance to double nuclei are briefly discussed. Centred anharmonic perturbations, with small non-axisymmetry are considered in § 4. § 5 is devoted to outlining the limits of applicability of the averaging principle, emergence of resonant families, and the outbreak of chaos. § 6 provides a summary of our results, paying some attention to the applicability of the averaging technique to M31 and NGC 4486B.

2 SLOW DYNAMICS

Consider a cluster of stars, orbiting around a BH located at the origin. The motion of a test star is determined by the Hamiltonian,

$$\mathcal{H} = \frac{v^2}{2} - \frac{GM}{r} + \Phi(\mathbf{r}) \quad (1)$$

where \mathbf{r} and \mathbf{v} are the position vector and velocity of the star, M is the mass of the BH, and Φ is the (time independent) mean gravitational potential of the cluster. Within the BH sphere of influence, Φ , by definition, is a small perturbation. Thus the orbits of stars (that are bound to the

[‡] It should be noted that σ itself is often not independent of distance from the BH. In this case, σ should be taken as the dispersion at $r = r_h$, which results in an equation wherein r_h is the unknown quantity to be solved for. Perhaps a better estimate of the sphere of influence of the BH is the radius at which the mass of the cluster equals the mass of the BH.

BH) may be thought of as Keplerian ellipses that precess and deform on time scales that are slow compared to orbital times. Hence it is useful to imagine that each star is a slowly precessing elliptical ring, with its mass distributed inversely proportional to its speed around its orbit—in the planetary context, this idea derives from Gauss (see Hagihara (1971) for a discussion of Gauss’s idea and its applications). Rauch and Tremaine (1996) introduced it to explore relaxation effects in star clusters around supermassive BHs. The elliptical ring approach emerges naturally in the averaging process discussed below.

When there is a separation of time scales, and one is interested in the slow evolution, it makes sense to average over high frequency variations: thus, time averages of physical quantities are equated to their space averages, an idea that has its roots in the works of Laplace, Lagrange and Gauss on planetary dynamics. Orbit-averaging has also been applied to study the evolution of the orbits of comets, perturbed by the Galactic tidal field (Heisler and Tremaine 1986). The straightforward way to achieve this is to express the problem in appropriate action-angle variables, identify the fast and (the two) slow angles, and integrate over the fast angle. Then the conjugate (fast) action is predicted to have no secular evolution. Laplace did this for the solar system, and concluded that the semi-major axes of the Keplerian ellipses of the planets do not evolve secularly. However, this is a reasonable approximation for the solar system only over times of order 10^4 yr . A major contribution to limiting the validity of averaging over orbital motions of the planets are mean motion resonances (i.e. “fast-fast” resonances). A natural worry is whether a similar phenomenon will afflict stellar dynamics in galactic nuclei. Let us consider nuclear star clusters in the collisionless limit, when there are an infinite number of stars contributing to a total finite mass for the cluster. Then each stellar orbit can be thought of as a being smoothly populated with stars. The gravitational force exerted by such an orbit on a test star will not display time variation on the orbital time scale (which would have obtained in the planetary case, when only one planet populates the orbit). Thus we expect no mean motion resonances in star clusters around nuclear BHs.[§] Resonances between fast and slow motions can be important for orbits with semi-major axes $\sim r_h$, and will stand in the way of this naive averaging procedure. Such resonances are the seeds of chaos, which we explore in § 5.

To apply the averaging principle, it is convenient to cast the Kepler problem in terms of the Delaunay action-angle variables: we write these as $(I, L, L_z; w, g, h)$, where (I, L, L_z) are action variables, and (w, g, h) are the respective conjugate angle variables.[¶] We list the basic definitions below, and refer the reader to text books (c.f. Plummer 1960,

[§] Of course, clusters might have as few as 10^6 stars, so that each orbit is not smoothly populated with stars. Hence there can be some discreteness noise, which would make the system somewhat collisional.

[¶] It is unfortunate that the notation employed by planetary dynamicists overlaps so heavily with those commonly used by galactic dynamicists for other physical quantities. Our notation is non standard, but we hope that it minimizes confusion.

Goldstein 1985) for the derivation.

$$\begin{aligned}
 I &= \sqrt{GMa}, \quad \text{where } a \text{ is the semi-major axis.} \\
 w &= \text{mean anomaly; marks time along Keplerian} \\
 &\quad \text{orbit—it is 0 at pericentre, and advances} \\
 &\quad \text{by } 2\pi \text{ in one circuit.} \\
 L &= \text{magnitude of the angular momentum; } L \leq I. \\
 g &= \text{angle from the ascending node to the pericentre.} \\
 L_z &= z\text{-component of angular momentum.} \\
 h &= \text{angle from } x\text{-axis to ascending node.} \quad (2)
 \end{aligned}$$

Expressed in the Delaunay variables, the Hamiltonian for the Kepler problem (equation 1 with Φ set equal to zero) assumes the simple form, $H_{\text{kep}} = -(G^2 M^2 / 2I^2)$. Thus w advances at a uniform rate,

$$\Omega(I) \equiv \left(\frac{dw}{dt} \right)_{\text{kep}} = \frac{\partial H_{\text{kep}}}{\partial I} = \frac{(GM)^2}{I^3}, \quad (3)$$

whereas the other five Delaunay variables remain constant.

Let us assume that we have managed to express Φ in terms of the new variables. Then the full Hamiltonian,

$$\mathcal{H} = -\frac{1}{2} \left(\frac{GM}{I} \right)^2 + \Phi, \quad (4)$$

where, with some abuse of notation, we now regard Φ as a function of all six Delaunay variables. For a general perturbation, the only conserved quantity is \mathcal{H} . The angles advance at rates given by

$$\frac{dw}{dt} = \Omega(I) + \frac{\partial \Phi}{\partial I}, \quad \frac{dg}{dt} = \frac{\partial \Phi}{\partial L}, \quad \frac{dh}{dt} = \frac{\partial \Phi}{\partial L_z}. \quad (5)$$

When Φ is small, Ω is the fastest frequency in the problem; thus w varies in time much faster than g and h , and averaging simply means that we can integrate the Hamiltonian of equation (4) over one circuit of w —this is equivalent to treating a star as an elliptical ring. The averaged Hamiltonian,

$$\begin{aligned}
 \overline{\mathcal{H}} &= \oint \frac{dw}{2\pi} \mathcal{H} = \oint \frac{d\eta}{2\pi} \left(1 - \sqrt{1 - (L/I)^2} \cos \eta \right) \mathcal{H} \\
 &= -\frac{1}{2} \left(\frac{GM}{I} \right)^2 + \overline{\Phi}, \quad (6)
 \end{aligned}$$

governs the slow dynamics of precessional motions. Since $\overline{\mathcal{H}}$ is independent of w , we recover Laplace's result that I is conserved by the slow dynamics. Furthermore, $\overline{\Phi}$ itself is another slow integral of motion.^{||} Without further ado, we can reach some general conclusions about slow dynamics in the region $r \ll r_h$. Below we list our conclusions in order of increasing generality:

- For razor-thin discs, motion is confined to the $z = 0$ plane. Any $\Phi(x, y)$ has the two slow integrals of motion, I and $\overline{\Phi}$. Hence the slow dynamics for two dimensional potentials, however non-axisymmetric or lop-sided, is integrable, and a straightforward classification of orbits is possible.

- For axisymmetric Φ in three dimensions, L_z is an exact integral of motion (since Φ is independent of h). We now

^{||} \mathcal{H} is, of course, exactly conserved, but this does not give us any extra conserved quantities after averaging.

have three integrals of motion (L_z , I and $\overline{\Phi}$), and the slow dynamics is again fully integrable.

- In three dimensions, when Φ has no symmetry whatsoever, we still have the integrals I and $\overline{\Phi}$. The slow motion can be chaotic, but it is clear that the chaos is limited.

2.1 Adiabatic growth of the BH

Averaging is also applicable to time dependent perturbations, $\Phi(\mathbf{r}, t)$, when the time variations are slower than the orbital times; as before, $I = \sqrt{GMa}$ is a quasi-invariant. In some scenarios of the formation and subsequent growth of the BH, its mass increases adiabatically (Peebles 1972, Young 1980); conservation of I implies that the semi-major axis shrinks in proportion to the growth of M . When the growth time is also much longer than the precessional timescales, additional (adiabatic) invariants might arise. These will, in general, be related to the actions corresponding to precessional degrees of freedom (L , L_z , g , h). We again consider cases with different spatial symmetry.

- For razor-thin discs, the conserved actions are I and $\oint L dg$, where the integral is performed at fixed time, over one cycle of motion in the $L - g$ plane.

- For three dimensional, axisymmetric cases, in addition to I and $\oint L dg$, we have L_z as an exactly conserved quantity.

- For configurations that have no spatial symmetry, I is in general the only conserved quantity, since resonances or precessional chaos might destroy the other adiabatic invariants.

It is difficult to make further progress without taking into account the self-consistent evolution of the cluster potential.

2.2 Slow planar dynamics

For razor-thin discs, orbits are restricted to the $x - y$ plane. (I, w) determine the semimajor axis and position on the orbit, and (L, g) the eccentricity and orientation of the ellipse in the plane. The only difference from the three dimensional case is that we allow L to take both \pm values. It proves convenient to set $w = \eta - e \sin \eta$, where η is the eccentric anomaly, and e is the eccentricity given by $e^2 = [1 - (L/I)^2] \leq 1$. If we imagine cartesian coordinates, (x', y') , centred at the origin, such that positive x' is along the major-axis toward the pericentre, and y' is parallel to the minor-axis, we have $x' = a(\cos \eta - e)$, and $y' = a\sqrt{1 - e^2} \sin \eta$. The primed coordinates being rotated by angle g with respect to the fixed coordinates, (x, y) , we obtain

$$\begin{aligned}
 x &= a \left\{ \cos g \left(\cos \eta - \sqrt{1 - \ell^2} \right) - \ell \sin g \sin \eta \right\} \\
 y &= a \left\{ \sin g \left(\cos \eta - \sqrt{1 - \ell^2} \right) + \ell \cos g \sin \eta \right\}, \quad (7)
 \end{aligned}$$

where $\ell = L/I$ is a dimensionless angular momentum which takes values, $-1 \leq \ell \leq 1$.

The frequency of apsidal precession of a test particle will depend on both the size (a) and shape (e) of the orbit. We wish to associate a characteristic value of this frequency, μ , with the size (but not the shape) of the orbit. Hence it

proves convenient to take μ to be of order the precession frequency for circular orbits (a somewhat paradoxical notion, but the limit is sensible). Then the ratio, $\delta(I) \equiv \mu(I)/\Omega$ is a convenient small parameter for slow dynamics. We now use a dimensionless time, $\tau = \mu t$, as an appropriate temporal measure for slow dynamics. Defining the dimensionless, averaged Hamiltonian,

$$H(\ell, g; I) = \frac{\bar{\Phi}}{I\mu} = \oint \frac{d\eta}{2\pi} \left(1 - \sqrt{1 - \ell^2} \cos \eta\right) \left(\frac{\Phi}{I\mu}\right), \quad (8)$$

the equations of motion take the standard form,

$$\dot{\ell} \equiv \frac{d\ell}{d\tau} = -\frac{\partial H}{\partial g}, \quad \dot{g} \equiv \frac{dg}{d\tau} = \frac{\partial H}{\partial \ell}. \quad (9)$$

In fact, much of the qualitative picture of the orbit families can be gleaned by studying the contour plot of H in the (g, ℓ) plane (for some value of the constant I).

2.3 A family of planar model potentials

To develop some analytic understanding of orbital structure, we introduce a family of planar potential perturbations that allow for both non-axisymmetry and lopsidedness.** Let us define a quadratic form,

$$q^2 = (x - d_1)^2 + \frac{(y - d_2)^2}{b^2}, \quad (10)$$

and the family of planar potentials,

$$\Phi(x, y) = \begin{cases} \text{sgn}(\alpha) \Phi_0 r_0^{-\alpha} (q^2 + r_c^2)^{\alpha/2}, & \alpha \neq 0; \\ (\Phi_0/2) \log(q^2 + r_c^2), & \alpha = 0, \end{cases} \quad (11)$$

The potentials depend on the five structural parameters, $(\mathbf{d}, r_c, b^2, c^2, \alpha)$, and a magnitude parameter $(\Phi_0 r_0^{-\alpha})$. The potentials are centred at a point that is displaced from the BH by $\mathbf{d} \equiv (d_1, d_2)$. Potential isocontours have a core of radius r_c , and constant axis ratio, b . The exponent α is a measure of the potential gradient across the contours; we require $2 \geq \alpha > -1$, a range that includes homogeneous cores as well as very centrally concentrated mass distributions. The potentials are lopsided for non zero \mathbf{d} , and are cuspy when $r_c = 0$. When both $\mathbf{d} = \mathbf{0}$ and $r_c = 0$, the dynamics itself is scale-free, so we may set $a = 1$. Lopsided potentials are not scale-free, even when $r_c = 0$; this is because the lopsidedness sets a scale (d). The magnitude, $(\Phi_0 r_0^{-\alpha})$ measures the slowness of the dynamics. Specifically, we choose units such that $\mu = (\Phi_0 a^\alpha / I r_0^\alpha) = (\Phi_0 a^\alpha / \sqrt{GMa} r_0^\alpha)$. As discussed above, the small parameter is $(\mu/\Omega) \propto a^{(1+\alpha)}$; since $\alpha > -1$, averaging is a very good approximation for small a .

** In the lopsided cases, the potential exerts a force on the BH, so we should imagine that the BH is ‘nailed’ down. It is possible to improve the situation by including cubic and higher order terms in the potential, but at the cost of considerably more complexity. We decided to forgo this luxury, since our primary goal in this paper is to pick out interesting orbits.

3 PLANAR HARMONIC PERTURBATIONS

The slow dynamics of *harmonic* perturbations, for which $\alpha = 2$, can be studied exactly for arbitrary non-axisymmetry, and lopsidedness. Pfenniger and de Zeeuw (1989) studied stellar orbits in the combined fields of a point mass, and a non-axisymmetric harmonic potential. For small energies they report that the orbits are essentially regular orbits in the Kepler potential of the point mass. As we demonstrate in this section, this is not quite true; the lenses and loops that emerge from our investigations are only *locally* Keplerian. They are better described as precessing and deforming Keplerian ellipses. They point out (correctly) the chaos that occurs for orbits with $a \sim r_h$, and discuss orbits of much higher energies. These are the orbits that will determine the overall shape of a galaxy, and they make the interesting point that, if the x and y frequencies of the harmonic potential are commensurate, then the high energy orbits will tend to stay well away from the centre, and hence avoid being strongly perturbed by the BH. We do not discuss their work any further, because our interest is dynamics within r_h .

The core radius loses dynamical significance in this case, so in our explorations of harmonic perturbations, we set $r_c = 0$:

$$\frac{\Phi}{I\mu} = \frac{1}{a^2} \left(d_1^2 + \frac{d_2^2}{b^2} - 2d_1x - 2\frac{d_2y}{b^2} + x^2 + \frac{y^2}{b^2} \right). \quad (12)$$

Substituting for x and y , the expressions given in equations (7), gives us the perturbation explicitly in terms of the Delaunay variables. We then average over w , and obtain the following expression for the slow Hamiltonian:††

$$H = -\frac{3}{2} \left(1 + \frac{\epsilon}{2}\right) \ell^2 - \frac{5\epsilon}{4} (1 - \ell^2) \cos 2g + 3\sqrt{1 - \ell^2} \left(\frac{d_1}{a} \cos g + (1 + \epsilon) \frac{d_2}{a} \sin g \right), \quad (13)$$

where we have introduced $\epsilon = (b^{-2} - 1)$ as a measure of non-axisymmetry. The parameter space is 3 dimensional, $(\epsilon, d_1/a, d_2/a)$, so that the slow dynamics of even planar, harmonic perturbations is quite rich. Below we study a few cases.

3.1 Centred harmonic perturbation: $d_1 = d_2 = 0$

The simplest case is a centred ($d_1 = d_2 = 0$) perturbation, for which we may without loss of generality, set $\epsilon \geq 0$. The Hamiltonian is

$$H = -\frac{3}{2} \left(1 + \frac{\epsilon}{2}\right) \ell^2 - \frac{5\epsilon}{4} (1 - \ell^2) \cos 2g, \quad (14)$$

and the equations of motion are,

$$\begin{aligned} \dot{\ell} &= -\frac{\partial H}{\partial g} = -\frac{5\epsilon}{2} (1 - \ell^2) \sin 2g \\ \dot{g} &= \frac{\partial H}{\partial \ell} = -3 \left(1 + \frac{\epsilon}{2}\right) \ell + \frac{5\epsilon}{2} \ell \cos 2g, \end{aligned} \quad (15)$$

†† A term, $[(5/2) + (5\epsilon/4) + (d_1/a)^2 + (1 + \epsilon)(d_2/a)^2]$, has been dropped in the slow Hamiltonian, because it does not contribute to slow dynamics.

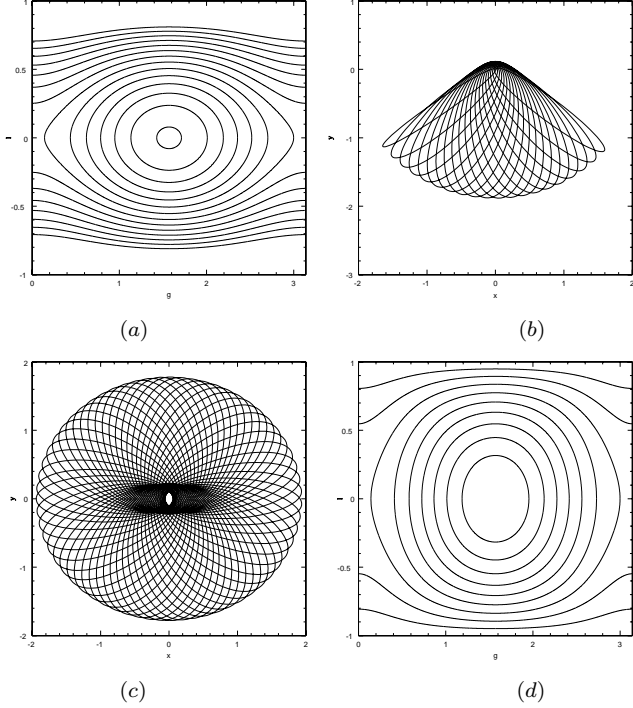


Figure 1. Planar, centred, harmonic perturbation: (a) isocontours of H in the (g, ℓ) plane for $\epsilon = 0.25$, (b) a lens orbit in real space corresponding to $H = -0.13$, (c) a loop orbit in real space corresponding to $H = -0.47$, (d) isocontours of H in the (g, ℓ) plane for $\epsilon = 1$

When $\epsilon = 0$, the full Hamiltonian is axisymmetric and the angular momentum is an exactly conserved quantity. The orbits are the rosette-like figures given in standard text books on classical mechanics. The averaged description, of course, coincides with this picture; $H = -3\ell^2/2$, the isocontours of which are simply lines of constant ℓ in the (g, ℓ) plane. These *loop* orbits are now viewed as Keplerian ellipses that precess at a rate, $\dot{g} = -3\ell$.

When $\epsilon \neq 0$, the non-axisymmetry gives birth to a new family of orbits, the *lenses*. Figure 1a shows contour plots of H for the case $\epsilon = 0.25$, for which the isocontours of the perturbation have axis ratio $b \simeq 0.9$. The lenses are parented by the short axis orbits, which appear as the stable fixed points located at $(\pi/2, 0)$ and $(3\pi/2, 0)$. Figure 1b shows a lens orbit (for $H = -0.13$); ℓ oscillates about zero, whereas g librates about the short axis. When $g = \pi/2$, it is maximally round, and when the pericentre reaches its maximum deviation from the short axis, the lens elongates to a line (“radial orbit”); its angular momentum now switches sign, and the orbit returns to maximal roundness at $g = \pi/2$, but with the opposite sign of ℓ . Unlike lenses, loops have a definite sign for ℓ , and g circulates through 2π in one period. The loop in Figure 1c is a deformed rosette that spends somewhat more time near the long axis, as it circulates around the origin. The unstable fixed points at $(0, 0)$ and $(\pi, 0)$ correspond to the long axis orbits. Loops are separated from lenses by the separatrix that straddles the unstable fixed points. The separatrix orbit, as well as the loops and lenses that are close to it spend a lot of time in the vicinity of the long axis. As

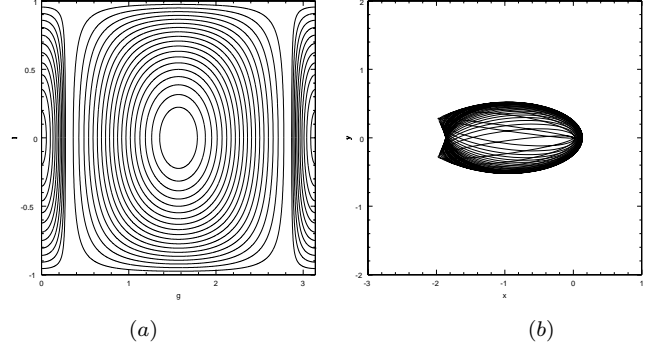


Figure 2. Planar, centred, harmonic perturbation: (a) isocontours of H for $\epsilon = 5.0$, (b) A long-axis lens orbit, for $H = -6.0$.

ϵ increases, lenses occupy an increasingly larger fraction of phase space (see Figure 1d).

When $g = n\pi$, equations (15) imply that $\dot{\ell} = 0$ and $\dot{g} = (\epsilon - 3)\ell$. Thus, when $\epsilon = 3$, $g = 0, \pi$ are *lines* of fixed points in the (g, ℓ) plane. In fact, when $\epsilon = 3$, the region occupied by the short-axis lenses has expanded to its fullest, squeezing the loops out of existence. This value of ϵ corresponds to axis ratio of two (for the isocontours of the harmonic perturbation), a case for which the full (unaveraged) Hamiltonian is exactly integrable (see Appendix A1 for details). For $\epsilon > 3$, loops are completely absent, and all of phase space is populated by lenses (see Figure 2a). The long-axis orbits now become stable, and parent families of *long-axis lenses*, one of which is shown in Figure 2b. We can demonstrate this change in stability of the long-axis orbit, by expanding the H of equation (14) to lowest order about the fixed point $(0, 0)$:

$$H = -\frac{5}{4}\epsilon + (\epsilon - 3)\frac{\ell^2}{2} + \frac{5\epsilon}{2}g^2. \quad (16)$$

When $\epsilon < 3$, the coefficients of ℓ^2 and g^2 are of opposite signs (the long-axis orbit is unstable), and have the same sign for $\epsilon > 3$ (when the long-axis orbit is stable). We can also see that the short-axis orbit remains stable by expanding H about $(\pi/2, 0)$. With $g = \pi/2 + \delta g$,

$$H = \frac{5}{4}\epsilon - (4\epsilon + 3)\frac{\ell^2}{2} - \frac{5\epsilon}{2}(\delta g)^2. \quad (17)$$

The coefficients of both ℓ^2 and $(\delta g)^2$ have the same sign, so the short-axis orbit is always stable.

3.2 Lopsided harmonic perturbation: $d_1 \neq 0$, $d_2 = 0$, $\epsilon = 0$

New orbits emerge when the centre of the perturbation is displaced from the BH. The simplest case occurs for $\epsilon = 0$, for which the isocontours of the perturbing potential are circles. In this case we may, without loss of generality, set $d_2 = 0$, and let $d_1 = d$. The Hamiltonian,

$$H = -\frac{3}{2}\ell^2 + 3\frac{d}{a}\sqrt{1 - \ell^2}\cos g. \quad (18)$$

now has a $(\cos g)$ term, which distinguishes between orbits that are *aligned* with, from those that are *anti-aligned* with the lopsidedness of the perturbation. We recall that g is the

angle from the major (x) axis to the pericentre of the instantaneous Keplerian ellipse. Thus orbits with $g = \pi$ are aligned, whereas $g = 0$ are anti-aligned with the lopsidedness. The only free parameter in H is d/a , which may be thought of as a dimensionless measure of lopsidedness. Below we explore the orbital structure as a function of this parameter.

The panels in Figures 3 show the dependence of the isocontours of H on lopsidedness. Changes in the topology of isocontours occur when d/a crosses 0.5 (Figure 3a to 3b), and again when d/a crosses unity (Figure 3c to 3d). This behavior is best understood by following the location and stability of the fixed points. The equations of motion are,

$$\begin{aligned}\dot{\ell} &= -\frac{\partial H}{\partial g} = 3\frac{d}{a}\sqrt{1-\ell^2}\sin g \\ \dot{g} &= \frac{\partial H}{\partial \ell} = -3\ell - 3\frac{d}{a}\frac{\ell}{\sqrt{1-\ell^2}}\cos g,\end{aligned}\quad (19)$$

and the fixed points are determined by requiring $\dot{\ell} = \dot{g} = 0$. There are four fixed points, located at

$$g = 0, \quad \ell = 0, \quad (\text{anti-aligned radial orbit});$$

$$g = \pi, \quad \ell = 0, \quad (\text{aligned radial orbit});$$

$$g = \pi, \quad \ell = \pm\sqrt{1-\frac{d^2}{a^2}}, \quad (\text{aligned loops}). \quad (20)$$

As Figures 3 show, the anti-aligned, radial orbit is a stable fixed point. The stability can be established by expanding H to lowest order about $(0, 0)$:

$$H = 3\frac{d}{a} - \frac{3}{2}\left(1 + \frac{d}{a}\right)\ell^2 - \frac{3d}{2a}g^2 + \dots \quad (21)$$

The coefficients of ℓ^2 and g^2 have the same sign, so the fixed point is stable.

When $d < 0.5a$ (see Figure 3a), the region of anti-aligned lenses, shares a border (a “separatrix” which goes through the origin of the $\ell - g$ plane) with rosette-like loops. These loops have a definite sense of circulation, anti-clockwise or clockwise according as ℓ is positive or negative. As the average value of $|\ell|$ increases, we sample this family of loops until we reach that rosette which at $g = 0$ has $|\ell| = 1$. This is a critical orbit, beyond which we enter the region occupied by the more interesting family of aligned loops, a family which we explore further down. As d increases to $0.5a$, the separatrix, which keeps apart anti-aligned lenses from rosettes, grows to its maximum allowable half-width of 1, squeezing the rosettes out of existence. As can be seen in Figure 3b, (for which $d/a = 0.6$), the rosettes have disappeared. The other fixed points correspond to orbits that are aligned with the lopsidedness. The aligned loops have eccentricity, $e = d/a$; they begin as circular orbits when $d = 0$, elongate with increasing lopsidedness, reducing to radial orbits when $d = a$. As discussed above, when $d/a < 0.5$, the aligned loops are separated from the anti-aligned lenses by the rosettes. As d/a increases beyond 0.5, and while $d/a < 1$, the family of aligned loops shrinks, and is now separated from the anti-aligned lenses by lens-like orbits surrounding the aligned radial orbit. All through this variation of d from 0 to $d = a$, the aligned radial orbit is unstable. At $d = a$, the two aligned loops (with either sign of ℓ) merge with the aligned radial orbit, which now remains stable for $d > a$. Again, this change of stability of the aligned, radial orbit

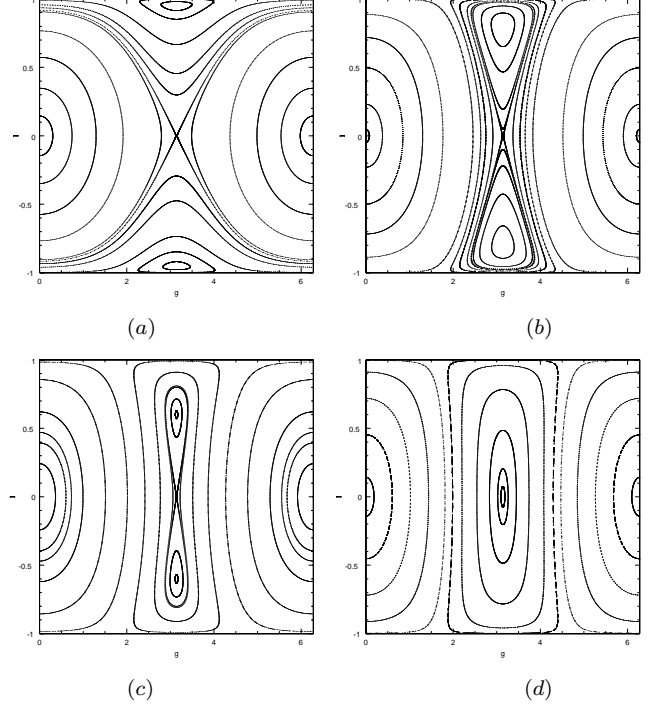


Figure 3. Isocontours of H for planar, lopsided, harmonic perturbation (a) $d = 0.3a$, (b) $d = 0.6a$, (c) $d = 0.8a$, (d) $d = 1.5a$.

may be verified by expanding the Hamiltonian about $(\pi, 0)$. Setting $g = \pi + \delta g$, to lowest order,

$$H = -3\frac{d}{a} - \left(1 - \frac{d}{a}\right)\frac{3\ell^2}{2} + \frac{3d}{2a}(\delta g)^2 + \dots \quad (22)$$

When $d < a$, the coefficients of ℓ^2 and $(\delta g)^2$ have opposite signs (fixed point unstable, but have the same sign for $d > a$ (fixed point stable). Hence there are three kinds of fixed points:

1. The anti-aligned radial orbit is stable for all d/a . This parents a family of *anti-aligned lenses* (see Figure 4a).
2. The aligned radial orbits are stable when $d > a$, and parents a family of *aligned lenses* (see Figure 4d).
3. The aligned loop orbits are stable when $d < a$. These parent a family of *librating loops*, to be discussed in some detail below.

There are no orbits that correspond to anti-aligned loops.

3.3 Possible applications to lopsided galactic nuclei

The aligned loops (which are fixed points of the slow dynamics) have constant angular momentum; ℓ is positive (negative) for anti-clockwise (clockwise) motion of the particle on its Keplerian ellipse. Their eccentricity, $e = d/a$, which means that the centres of the ellipses coincides with the centre of the perturbation (the BH is at one of the foci). For a fixed value of d , aligned loops of varying sizes (i.e. a), form a family of concentric, confocal ellipses. Not only can stars be placed on such orbits, but being a non-intersecting family, such nested ellipses can also be the streamlines of gas flows. Figure 5a shows one such representative set of aligned loops.

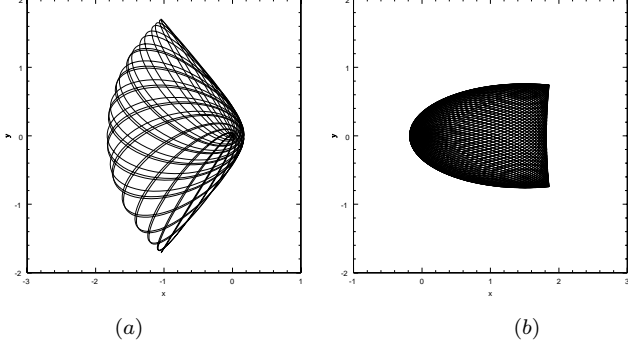


Figure 4. Lens orbits for the planar, lopsided, harmonic perturbation: (a) an anti-aligned lens orbit for $a = 1$, $d = 0.5$, (b) an aligned lens orbit for $a = 1$, $d = 1.5$.

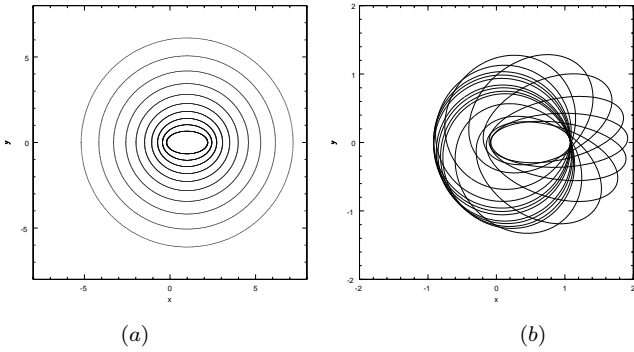


Figure 5. Loop orbits for the planar, lopsided, harmonic perturbation: (a) a set of aligned-loops when $d = 1$. The ten nested ellipses have $a = 1.2, (1.2)^2, \dots, (1.2)^{10} \simeq 6.19$, (b) A librating loop for $d = 0.5$, $a = 1$, for which ℓ fluctuates between 0.4 and 0.97.

Stable oscillations about these fixed point orbits allows ℓ to oscillate, while preserving a definite \pm sign. Unlike the circulating loops of the centred perturbation (see Figure 1c), g for one of these *librating loops* oscillates about its mean value of π (see Figure 5b).

Tremaine (1995) has suggested that the nucleus of M31 is an eccentric disc in which stars move on nearly Keplerian orbits around a massive BH. In his model, the location of the BH coincides with the fainter (brightness) peak, P2, and brighter peak, P1, is the apoapsis region of the Keplerian ellipses. If we imagine that the lopsided harmonic perturbation mocks self-gravity, our toy model suggests that the orbits such as our aligned loops (and their progeny, the librating loops) might form the backbone of star clusters such as Tremaine’s eccentric discs.

4 CENTRED PERTURBATIONS FOR GENERAL α

When $\alpha \neq 2$, it is no longer possible to obtain exact expressions for the slow Hamiltonian. One possibility is to evaluate H numerically, and study the contour plots. Another option is to look at limiting cases, which is what we do below. In this Section we study centred, nearly circular perturbations: $d_1 = d_2 = 0$ and $0 < \epsilon \ll 1$. Equation (11), for $\alpha \neq 0$, gives

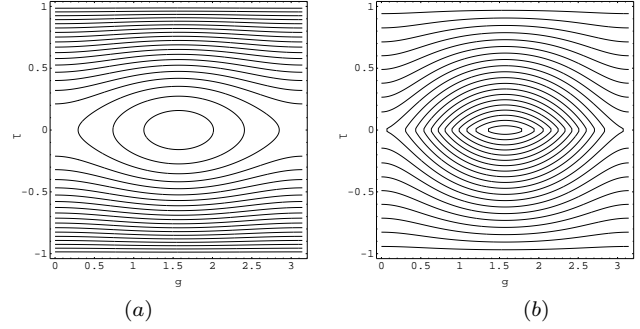


Figure 6. Isocontours of H for $\epsilon = 0.1$ (accurate to first order in ϵ): (a) $\alpha = 1$, (b) $\alpha = -0.9$.

us the following scale-free potentials:

$$\begin{aligned} \frac{\Phi(x, y)}{\mu I} &= \frac{1}{a^\alpha} (x^2 + (1 + \epsilon)y^2)^{\alpha/2} = \frac{1}{a^\alpha} (r^2 + \epsilon y^2)^{\alpha/2} \\ &= \left(\frac{r}{a}\right)^\alpha + \epsilon \frac{\alpha}{2} \left(\frac{r}{a}\right)^{\alpha-2} \left(\frac{y}{a}\right)^2 + O(\epsilon^2). \end{aligned} \quad (23)$$

We can now substitute in equation (23), the following expressions,

$$\begin{aligned} r &= a \left(1 - \sqrt{1 - \ell^2} \cos \eta\right), \\ y &= a \left\{ \sin g \left(\cos \eta - \sqrt{1 - \ell^2}\right) + \ell \cos g \sin \eta \right\}, \end{aligned} \quad (24)$$

for r and y , and average over η to obtain the averaged Hamiltonian (see Appendix A2 for the derivation) correct to first order in ϵ :

$$\begin{aligned} H(\ell, g; \alpha, \epsilon) &= \left(1 + \frac{\epsilon\alpha}{4} - \frac{\epsilon\alpha}{4} \cos 2g\right) \times \\ &\times F\left(-\frac{1+\alpha}{2}, -\frac{\alpha}{2}, 1, 1 - \ell^2\right) \\ &+ \frac{\epsilon\alpha}{4} \ell^2 \cos 2g \times \\ &\times F\left(\frac{1-\alpha}{2}, \frac{2-\alpha}{2}, 2, 1 - \ell^2\right), \end{aligned} \quad (25)$$

where F is Gauss’ Hypergeometric function. When $\alpha = 1$ or 2, the Hypergeometric series for F terminates, and the Hamiltonian assumes a simple form. We have already discussed the case $\alpha = 2$ in some detail.^{‡‡} When $\alpha = 1$,

$$\begin{aligned} F\left(-1, -1/2, 1, 1 - \ell^2\right) &= \frac{3 - \ell^2}{2}, \\ F\left(0, 1/2, 2, 1 - \ell^2\right) &= 1, \end{aligned} \quad (26)$$

so that

$$H(\ell, g; 1, \epsilon) = \left(\frac{1}{2} + \frac{\epsilon}{8}\right) (3 - \ell^2) - \frac{3\epsilon}{8} (1 - \ell^2) \cos 2g, \quad (27)$$

to first order in ϵ . Figure 6a shows the isocontours of this Hamiltonian ($\alpha = 1$) for $\epsilon = 0.1$; as may be seen, these are similar to those of Figure 1a. Keeping ϵ small, we can vary α from -1 to 2. Figure 6b shows the isocontours for $\alpha = -0.9$;

^{‡‡} For $\alpha = 2$, equation (25) reduces to equation (14), which happens to be an exact expression, because terms of $O(\epsilon^2)$ are identically zero for this case.

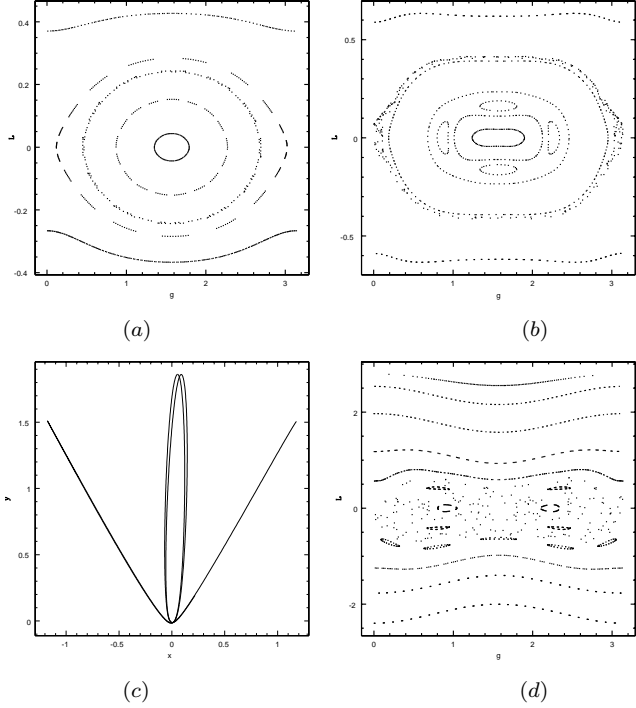


Figure 7. Dynamics in the potential of a black hole perturbed by a logarithmic potential with $b = 0.9$: (a) Section on energy surface with zero velocity orbit $y = 0$ and $x = 0.8r_h$; (b) similar section but with $x = 2.0r_h$; (c) Periodic orbit at the centre of the chain of islands seen in (b); (d) Section on energy surface with zero velocity orbit $y = 0$ and $x = 4.0r_h$.

again the overall structure is unchanged. Hence we conclude that, for small ϵ , the orbital structure is independent of α in the range $(-1, 2)$, with loops and short-axis lenses broadly similar to those in Figures 1b and 1c.

5 THE LIMITS OF AVERAGING

The averaged Hamiltonian is an accurate proxy for the full Hamiltonian when the orbital period is much shorter than the period of precession of periaapse. Such is mostly the case for orbits that reside within the sphere of influence of the BH. However as one moves outwards, the influence of the perturbations relative to the BH’s pull increases, the mismatch in frequencies decreases, thereby invalidating the averaging procedure. In practice, the breakdown occurs at resonances between orbital and precessional motion and is responsible for the emergence of minor orbit families such as the ones discussed by Gerhard and Binney (1985) and Miralda-Escude and Schwarzschild (1989)—hereafter GB and MES, respectively.

In what follows, we display the gradual breakdown of averaging as one moves away from a BH of mass M , in the scale-free logarithmic potential of MES:

$$\Phi(x, y) = \frac{v_L^2}{2} \ln \left(x^2 + \frac{y^2}{b^2} \right), \quad (28)$$

where v_L is the characteristic velocity of large loops, and b is a measure of non-axisymmetry. The dynamics being two dimensional, we can explore the phase space structure on a

Poincare section. Since we are interested in resonances between orbital and precessional motions, we choose to strobe the dynamics with the orbital period at each apocentre passage, recording the angular momentum, L , and the argument of the pericentre, g .

MES studied the scale-free case thoroughly. The phase space is divided between orbits with a definite sense of circulation (librating non-aligned loops and rosettes) and those with no definite sense of circulation. The latter are broken into resonant orbit families: banana, fish, pretzel...etc. The resonances are between the orbital period of the star and the period of precession of its pericentre. The banana for instance, performs two orbital revolutions in the time it takes its pericentre to precess once. Such resonances are naturally missed by the averaged Hamiltonian which assumes that the orbital period is much faster than the precessional period (see Touma and Tremaine (1997) for a discussion of the averaged Hamiltonian).

We now place a BH at the origin and study the restructuring of orbits that occurs. MES did introduce a BH but did not show any surface of section. They presented samples of high energy orbits, including some regular ones. The BH radius of influence is given by, $r_h = GM/v_L^2$. We measure distance in units of r_h , and look at sections of increasing energy. The energy is that of an orbit with zero velocity started on the x -axis, with $x = fr_h$, $f = 0.4, 2.0, 4.0$.

Within r_h (Figures 7a), the phase space is occupied by two main families of regular orbits: short axis lenses and loops. The lenses appear naturally in the integrable cusps with BHs presented in Sridhar and Touma (1997). The apparent integrability of the motion is consistent with the validity of averaging at distances where the motion is dominated by the BH. The phase space of the corresponding averaged Hamiltonian was not described in this paper, but it hardly differs from the averaged dynamics of centered harmonic perturbations discussed above (this should be obvious from the results of § 4). As one moves out in radius past r_h (Figure 7b), resonances become stronger, and a layer of stochastic motion develops near the separatrix. A torus has broken up into a chain of islands. The corresponding resonant periodic orbit, the bowtie, is shown in Figure 7c. Further away from the BH (Figure 7d), the short axis radial orbit becomes unstable, bananas are born, together with other resonant orbit families which overlap and lead to large scale chaos where once the regular lens orbits lived.

GB studied the logarithmic potential with core and BH. They were mostly interested in energetic orbits far outside r_h and they find that resonant orbit families and stochastic orbits dominate the phase space. When commenting on dynamics inside r_h , they just mention that most orbits are loops which, as we now know, is incomplete. In fact, within r_h , the dynamics is accurately described by the integrable, orbit averaged Hamiltonian; the phase space is regular with mainly short axis lenses and loops. As one moves outside the sphere of influence, lenses and loops break down into resonant orbit families, which get stronger, overlap and lead to stochastic orbits. The short axis radial orbit goes unstable and regular lens orbits disappear, as the region within the separatrix is practically engulfed by a single stochastic orbit. GB described stochasticity in terms of scattering of box orbits by the central cusp and BH. Here, stochasticity

emerges with the gradual sacrifice of regular lens orbits to strong overlapping resonances as we move away from the BH.

6 DISCUSSION

In this paper we have introduced an averaging technique into the study of star clusters around massive BHs at the centres of galaxies. The dynamics of these clusters is governed by the combined gravitational potential of the central BH and the cluster itself. Within the sphere of influence (r_h) of the BH, the cluster potential is a small, yet non negligible perturbation. Orbits that are confined within r_h may be viewed as slowly precessing (and deforming) Keplerian ellipses. We have shown that these orbits possess a quasi-integral of motion, in addition to the energy integral; this nearly conserved quantity is $I = \sqrt{GMa}$, where M is the mass of the BH, and a is the semimajor axis of the orbit (when M is constant, the semimajor axis is nearly conserved). The quasi-integral arises because the Keplerian orbital frequency is much larger than the frequencies of precessional motions. Taking advantage of this mismatch in frequencies, we averaged over an orbital period, to obtain a reduced dynamics of slow, precessional motions, wherein I appears as a full-fledged integral of motion.

The building of self-consistent stellar models for systems with low spatial symmetry (such as the central regions of M31 and NGC 4486B, which are known to possess double nuclei) surely requires the existence of more than one integral of motion. We now have in hand two integrals of motion—the energy and the semimajor axis—that may be used to construct dynamical models for the centres of galaxies like M31 and NGC 4486B. Let us verify that the conditions required for the averaging to apply are met in these two cases.

1. M31 probably has a central BH of mass $\sim 6 \times 10^7 M_\odot$. For velocity dispersion $\sim 160 \text{ km s}^{-1}$, $r_h \sim 10 \text{ pc}$ ($\sim 3''$). The double nuclei are separated by $\sim 0.''5$ arcsec, and much of the nuclear disc itself appears to be within r_h . Furthermore, within $1''$, the mass of the disc and the bulge are only 16 %, and 2 % of the mass of the BH respectively (see Tremaine 1995). Within r_h , the gravitational potentials of the disc and the bulge are small, but non negligible, perturbations to the potential of the BH; indeed, this is a situation that is ripe for the application of the averaging technique! In § 3.2 and 3.3, we considered orbits in a toy model of a lopsided perturbation, and discovered that there are a very interesting class of loop orbits that are elongated in the same sense as the perturbation. The existence of these aligned loop orbits is an encouraging sign that Tremaine's (1995) eccentric disc can be realised as a self-consistent model.

2. NGC 4486B (a low luminosity E1 companion of M87) also has a double nucleus separated by $0.''15$ (Lauer et.al. 1996). There seems to be some evidence for a central BH of mass $\sim 9 \times 10^8 M_\odot$ (Kormendy et. al. 1997). For a velocity dispersion $\sim 175 \text{ km s}^{-1}$, and an assumed distance to NGC 4486B of 16 Mpc, we estimate that $r_h \sim 1.''6$, a length scale that is not only larger than the separation between the nuclear peaks, but also one that is nearly fifteen times larger than the best resolution obtainable with the HST; hence the averaging technique may be expected to be useful here too. Kormendy et. al. (1997) suggest that the double nucleus

might arise from a stellar distribution similar to Tremaine's (1995) disc. However, as Lauer et.al. (1996) note, there are differences from the case of M31, and even the evidence for a massive BH is less certain.

A fundamental result of this paper is that the presence of a massive BH enforces a certain degree of integrability within its sphere of influence; and this happens because of the existence of the secular invariant, I . Even without detailed knowledge of the (perturbing cluster) potential, we were able to note that slow dynamics in (i) razor-thin discs is fully integrable because the problem is two dimensional, (ii) any axisymmetric potential is fully integrable (note that axisymmetry allows for lopsidedness), and (iii) a potential with no spatial symmetry whatsoever still conserves two integrals, so that any precessional chaos must be highly limited in nature.

When the potential is time dependent, but with variations occurring over times longer than the orbital times, averaging is still applicable. We discussed the case of the adiabatic growth of the BH. Another case of slow time variation comes to mind: this is the 'resonant relaxation' of Rauch and Tremaine (1996), a process that relies on two body encounters between stars. The time scales are typically much longer than orbital times, so averaging applies, and the stars in their courses may be treated as elliptical rings. Over certain time scales (shorter than the classical two body relaxation times), the semimajor axes of all the stars are approximately constant, whereas torques between the rings exchange angular momentum. As the authors note, this can lead to a situation in which some regions of nuclear star clusters are relaxed in angular momentum, but not in energy.

We introduced a family of model planar potentials, that allow for a range of cusp slopes (α), non-axisymmetry and lopsidedness, with a view to classification of orbit families. For the harmonic case ($\alpha = 2$), we showed that centered non-axisymmetric perturbations support two main families of orbits: short axis lenses and loops. Lenses were introduced in Sridhar and Touma (1997) and should be recognized as an essential feature of regular motion around BHs. They have zero average angular momentum and fill out lens shaped regions in configuration space. The loops are the familiar rosettes of slightly perturbed Keplerian motion. We explored the consequences of lopsidedness and identified a family of (resonant) aligned loops whose elongation is in the same sense as the lopsidedness.

When $\alpha \neq 2$, the case of small non-axisymmetry ($\epsilon \ll 1$) is analytically tractable. The qualitative nature of the orbits (lenses and loops) appears to be insensitive to α . This is probably because the force exerted on a star due to the perturbing potential—even when it becomes infinitely large at the centre—is overwhelmed by the force due to the BH. If such is the case for larger non-axisymmetry, then our explorations of the harmonic case provide a sketch of the possible orbit families in razor-thin discs around massive BHs. Whether the qualitative nature of dynamics around BHs is indeed independent of the steepness of the cusp in density is an unsolved problem, but one that is tractable by methods such as our averaging technique.

Averaging is of course valid as long as we are far away from resonances between the orbital period and the periods of apsidal or nodal precession. We showed, numerically,

that such a condition is indeed satisfied for $r < r_h$, but breaks down outside. Orbits which take a star far outside r_h may be expected to be chaotic (c.f. (Gerhard & Binney (1985)), (Merritt (1997))). Central BHs and strong cusps might force the main body on an elliptical galaxy to evolve toward axisymmetry. However, as we have argued in this paper, the central regions of galaxies might stubbornly persist with their striking variety of non-axisymmetric features.

7 ACKNOWLEDGMENTS

We thank the Raman Research Institute, and the Indian Railways for their hospitality while this work was in progress. JT wishes to thank IUCAA for support and hospitality at Pune, as well as acknowledge the support of the Harlan Smith Fellowship under NASA grant NAGW 1477.

APPENDIX A: THE CASE $\epsilon = 3$

We show that even the *unaveraged* dynamics, in the combined potential of a BH and a centered harmonic perturbation, is integrable, when $\epsilon = 3$ (i.e. $b = 0.5$). Indeed the combined potential,

$$\Phi = -\frac{GM}{\sqrt{x^2 + y^2}} + K(x^2 + 4y^2), \quad (\text{A1})$$

when expressed in parabolic coordinates (see Sridhar and Touma 1997 for details), $\xi = y + \sqrt{x^2 + y^2}$, and $\eta = y - \sqrt{x^2 + y^2}$, takes the form

$$\Phi = \frac{F_+(\xi)}{\xi - \eta} + \frac{F_-(\eta)}{\eta - \xi}, \quad (\text{A2})$$

where

$$\begin{aligned} F_+(\xi) &= K(\xi^3 - GM) \\ F_-(\eta) &= K(-|\eta|^3 + GM). \end{aligned} \quad (\text{A3})$$

This form is that of a separable, Stäckel potential in parabolic coordinates, which supports integrable motion.

APPENDIX B: HAMILTONIAN FOR GENERAL α

Let Φ denote the potential given in equation (23). Substitute for r and y , the expressions given in equations (24), and average over η in the usual manner. This gives us the averaged Hamiltonian, $H = (\overline{\Phi}/\mu I) = H_0 + \epsilon H_1 + O(\epsilon^2)$, where

$$\begin{aligned} H_0 &= \frac{1}{2\pi} \oint d\eta \left(1 - \sqrt{1 - \ell^2} \cos \eta\right)^{\alpha+1}, \\ H_1 &= \frac{\alpha}{4\pi} \oint d\eta \left(1 - \sqrt{1 - \ell^2} \cos \eta\right)^{\alpha-1} \times \\ &\quad \times \left\{ \sin g \left(\cos \eta - \sqrt{1 - \ell^2}\right) + \ell \cos g \right\}^2. \end{aligned} \quad (\text{B1})$$

Some straightforward algebra allows us to express

$$H = \left(1 + \frac{\epsilon\alpha}{4}\right) A(\ell; \alpha) - \frac{\epsilon\alpha}{4} B(\ell; \alpha) \cos 2g + O(\epsilon^2), \quad (\text{B2})$$

in terms of the two functions, A and B :

$$\begin{aligned} A(\ell; \alpha) &= F\left(-\frac{1+\alpha}{2}, -\frac{\alpha}{2}, 1, 1 - \ell^2\right), \\ B(\ell; \alpha) &= A - \ell^2 F\left(\frac{1-\alpha}{2}, \frac{2-\alpha}{2}, 2, 1 - \ell^2\right), \end{aligned} \quad (\text{B3})$$

where we have used formulae 3.666, 8.703 and 9.131 (1) of Gradshteyn and Ryzhik (1994). Substituting for A and B in equation (B2) completes the derivation.

REFERENCES

- Gebhardt, K., et. al., 1996, AJ, 112, 105
 Gerhard, O. E., & Binney, J., 1985, MNRAS, 216, 467
 Goldstein, H., 1980, Classical Mechanics, 2nd ed. (Reading: Addison-Wesley)
 Gradshteyn, I. S., and Ryzhik, I. M., 1994, Table of Integrals, Series, and Products, edited by A. Jeffrey (Academic Press, Inc, Boston)
 Hagihara, Y., 1971, Celestial Mechanics II, Part I (MIT Press, Cambridge, Ma)
 Heisler, J. and Tremaine, S., 1986, Icarus, 65, 13
 Kormendy, J., 1982, in Morphology and Dynamics of Galaxies, edited by L. Martinet and M. Mayor (Geneva Observatory, Sauverny), p 113
 Kormendy, J., 1987, in Structure and Dynamics of Elliptical Galaxies, IAU Symposium No. 127, edited by T. de Zeeuw (Reidel, Dordrecht), p 17
 Kormendy, J., & Richstone, D., 1995, ARAA 33, 581
 Kormendy, J., et. al., 1997, ApJ, 482, L139
 Lauer, T.R., 1983, Ph.D thesis, University of California, Santa Cruz
 Lauer, T.R., 1985, ApJ, 292, 104
 Lauer, T.R. et. al. 1993, AJ, 106, 1436
 Lauer, T.R., et. al., 1995, AJ, 110, 2622
 Lauer, T.R., et. al., 1996, ApJ, 471, L79
 Merritt, D., 1997, ApJ, 486, 102
 Merritt, D., 1998, Comments on Astrophysics, 19
 Miralda-Escudé, J., & Schwarzschild, M., 1989, ApJ 339, 752
 Peebles, P.J.E., 1972, Gen. Rel. Grav., 3, 61
 Pfenniger, D. & de Zeeuw, T., 1989, in Dynamics of Dense Stellar Systems, edited by D. Merritt (Cambridge University Press, Cambridge), 81
 Plummer, H. C., 1960, An Introductory Treatise on Dynamical Astronomy (Dover, New York)
 Rauch, K.P., & Tremaine, S., 1996, New Astronomy, 1, 149
 Rees, M.J., 1990, Science, 247, 817
 Sridhar, S., & Touma, J., 1997, MNRAS 287, L1-L4
 Touma, J. & Tremaine, S., 1997, MNRAS 292, 905
 Tremaine, S., 1995, AJ, 110, 628
 Young, P., 1980, ApJ, 242, 1232